Available online at www.sciencedirect.com
ScienceDirect
Journal of Power Sources 164 (2007) 668–677
JOURNAL OF POWER SOURCES
www.elsevier.com/locate/jpowsour

Internal shorting and fuel loss of a low temperature solid oxide fuel cell with SDC electrolyte

Xinge Zhang *, Mark Robertson, Cyrille Decês-Petit, Wei Qu, Olivera Kesler, Radenka Maric, Dave Ghosh

Institute for Fuel Cell Innovation, National Research Council Canada, 4250 Wesbrook Mall, Vancouver, BC V6T 1W5, Canada

Received 15 August 2006; received in revised form 27 October 2006; accepted 31 October 2006
Available online 5 December 2006

Abstract

A solid oxide fuel cell with $Sm_{0.2}Ce_{0.8}O_{1.9}$ (SDC) electrolyte of 10 μm in thickness and Ni–SDC anode of 15 μm in thickness on a 0.8 mm thick Ni–YSZ cermet substrate was fabricated by tape casting, screen printing and co-firing. A composite cathode, 75 wt.% $Sm_{0.5}Sr_{0.5}CoO_3$ (SSCo) + 25 wt.% SDC, approximately 50 μm in thickness, was printed on the co-fired half-cell, and sintered at 950 °C. The cell showed a high electrochemical performance at temperatures ranging from 500 to 650 °C. Peak power density of 545 mW cm^{-2} at 600 °C was obtained. However, the cell exhibited severe internal shorting due to the mixed conductivity of the SDC electrolyte. Both the amount of water collected from the anode outlet and the open circuit voltage (OCV) indicated that the internal shorting current could reach 0.85 A cm^{-2} or more at 600 °C. Zr content inclusions were found at the surface and in the cross-section of the SDC electrolyte, which could be one of the reasons for reduced OCV and oxygen ionic conductivity. Fuel loss due to internal shorting of the thin SDC electrolyte cell becomes a significant concern when it is used in applications requiring high fuel utilization and electrical efficiency.

Keywords: SOFC; Low temperature; SDC; Internal shorting; Fuel loss

1. Introduction

Solid oxide fuel cells (SOFC) have been recognized as a promising energy conversion technology in terms of cleanliness, efficiency and ability to work with various fuels. During the last decade, nickel–yttria stabilized zirconia (Ni–YSZ) anode supported solid oxide fuel cells (SOFCs) with thin film electrolytes have been widely adopted by industrial pioneers and research groups throughout the world. Encouraging performance in the intermediate temperature range (700–800 °C) with thin film YSZ electrolytes has been achieved [1]. However, a high degradation rate in stack performance has been observed, which is unacceptable for commercial application [2]. Thermally activated material degradation, in particular, high temperature corrosion of Fe–Cr steel interconnects, has been identified as a serious problem [2,3]. To date, extensive R&D efforts are focusing on decreasing cell operating temperatures below 600 °C in order to expand lifetime and to reduce the cost of SOFCs [4–7].

The practical operating temperature of an SOFC is mainly determined by the conductivity and thickness of the electrolyte. Doped ceria is a promising option for an electrolyte material for low temperature use. It has an ionic conductivity that is two to three times higher than that of YSZ. Its thermal expansion coefficient (12.5×10^{-6} K^{-1}) is much closer to that of the Ni–cermet substrate and commercial ferritic stainless steel interconnects, compared with YSZ (10.5×10^{-6} K^{-1}). Moreover, it has better chemical compatibility with high performance cobalt-containing cathodes, such as $Sm_{0.5}Sr_{0.5}CoO_3$ [4,8], $La_{0.6}Sr_{0.4}Co_{0.2}Fe_{0.8}O_3$ [9] and $Ba_{0.5}Sr_{0.5}Co_{0.2}Fe_{0.8}O_3$ [10]. A maximum power density of 1 W cm^{-2} at 600 °C with an anode-supported thin ceria based electrolyte cell has been reported [10]. The main disadvantage of a ceria-based electrolyte is that it becomes a mixed conductor in anodic conditions, which causes cell voltage loss and fuel efficiency loss due to internal shorting. Chemical and mechanical stability, thermal cycle capability and redox tolerance are also other concerns for long-term service.

* Corresponding author. Tel.: +1 604 221 3077; fax: +1 604 221 3001.
E-mail address: xinge.zhang@nrc.gc.ca (X. Zhang).

0378-7753/$ – see front matter © 2006 Elsevier B.V. All rights reserved.
doi:10.1016/j.jpowsour.2006.10.087

Table 1
Chemical composition, properties and supplier of starting materials

Material for	Composition	Properties	Supplier
Cathode	$Sm_{0.5}Sr_{0.5}CoO_3$ (SSC)	D50, 0.80 μm; surface area, 5.16 $m^2\ g^{-1}$	Praxair
Electrolyte	$(SmO_{1.5})_{0.2}(CeO_2)_{0.8}$ (SDC)	D50, 0.40 μm; surface area, 7.08 $m^2\ g^{-1}$	Praxair
Anode	NiO (type F)	D50, 1.0 μm; surface area, 4.0 $m^2\ g^{-1}$	Novamet
Cermet substrate	NiO (standard)	D50, 16.0 μm; surface area, <1 $m^2\ g^{-1}$	Novamet
	8YS (YSZ)	D50, 0.520 μm; surface area, 6.2 $m^2\ g^{-1}$	Tosoh

In the present work, an anode supported, thin SDC electrolyte cell was used for internal shorting and fuel loss investigations. It was found that although the cell showed a fairly high maximum power density of 545 mW cm^{-2} at 600 °C, it also showed severe internal shorting due to the mixed conductivity of the SDC electrolyte of the cell. Fuel loss due to internal shorting of the thin SDC electrolyte cell could impede its use in practical applications requiring high fuel efficiency.

2. Experimental procedure

2.1. Cell fabrication

A NiO–YSZ cermet substrate supported $Sm_{0.2}Ce_{0.8}O_{1.9}$ (SDC) electrolyte SOFC was used. Table 1 lists the starting ceramic powder materials for cell fabrication. All the materials are commercially available. Fig. 1 shows a schematic diagram of the cell structure, which consists of a NiO–YSZ cermet substrate (0.8 mm), NiO–SDC anode layer (15 μm), SDC electrolyte (10 μm) and SSCo#3 composite cathode (50 μm). A 57 wt.% NiO + 43 wt.% YSZ powder mixture was used for the NiO–YSZ cermet substrate. The composition of the NiO–SDC anode was 53 wt.% NiO + 47 wt.% SDC. The SSCo#3 composite cathode consists of 75 wt.% $Sm_{0.5}Sr_{0.5}CoO_3$ (SSC) and 25 wt.% SDC. The cell was fabricated by tape-casting the substrate, screen-printing the anode and then the electrolyte on the substrate tape and co-firing at 1400 °C for 2 h, followed by cathode printing and sintering at 950 °C for 2 h. Further details about the cell fabrication process can be found in ref. [21]. The cell used in this study was 27.5 mm in diameter. The edge of the cell was sealed with alkaline borosilicate glass (Corning #0211, treated at 750 °C). The SDC electrolyte after glass sealing has an effective area of 5.23 cm^2. The SSCo#3 cathode area was 1.35 cm^2. In this paper, cells with and without cathodes were investigated.

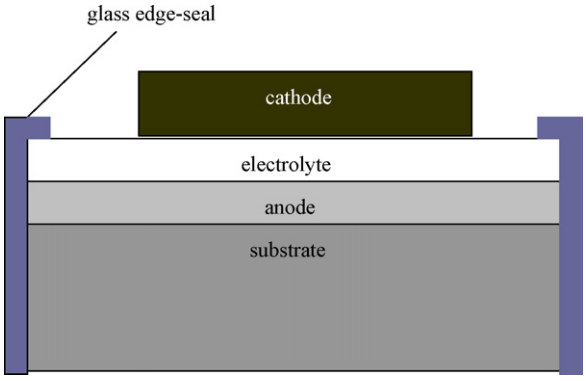

Fig. 1. Schematic of cell structure.

2.2. Cell characterization

The 1400 °C sintered electrolytes appear transparent, crack-free and allow no detectable helium gas cross-leakage at 13.8 kPa (approximately 2 psi), indicating that the electrolyte layers were fully dense. The measured cell density (by an Archimedes density measurement) is 5.20 g cm^{-3}, which corresponds to 18.2% porosity in the NiO–YSZ cermet substrate based on the cermet substrate composition of 57.0 wt.% NiO. The substrate porosity would be increased to approximately 36.4% porosity after NiO reduction to Ni. The porosity of the SSCo#3 cathode is approximately 40% after sintering at 950 °C.

Fig. 2 shows a schematic setup for button cell electrochemical tests. A split-tube furnace (Thermcraft incorporated) was used for cell temperature control. The thermocouple for furnace temperature control was located near the cell at the anode side (T_a). There were also two additional thermocouples, one located in the furnace chamber for overheating protection (T_f), and the other contacting the electrolyte surface of the cell at the cathode side (T_c). The cells were mounted for electrochemical testing at the end of an alumina tube with inner diameter of 18 mm, and sealed with a borosilicate glass seal at the anode side. A thin layer of cathode paste was applied to the cell cathode to create a good contact between the cathode and the cathode current collector (Pt mesh) in the testing apparatus. A constant spring loaded force was applied to the cathode air supply alumina tube, of approximately 1.5 kg force. The cell was heated up to 750 °C at a ramp rate of 180 °C h^{-1}, and held for 12 h for glass seal softening and crystallization to reach an anodic hermetic sealing as well as cathodic contact paste in situ sintering. The temperature was then decreased to 650 °C for anode reduction and cell electrochemical measurements. Ambient air was introduced at a flow rate of 100 ml min^{-1} to the cathode side. During the cell reduction, a combination of nitrogen and hydrogen as anode gas at the total flow rate of 100 ml min^{-1} was first passed through a bubbler-type humidifier at room temperature, corresponding to approximately 3% H_2O content and then introduced to the anode side. The gas combination used five different hydrogen concentrations during the cell reduction process: 10% H_2 for 0.5 h, 20% H_2 for 0.5 h, 40% H_2 for 1 h, 60% H_2 for 0.5 h and finally 100% H_2. The outlet of the anode gas was passed through a bottle at room temperature before being vented. After the cell reduction and performance test, the water produced during reduction and (or) performance test was discarded. The anode outlet was

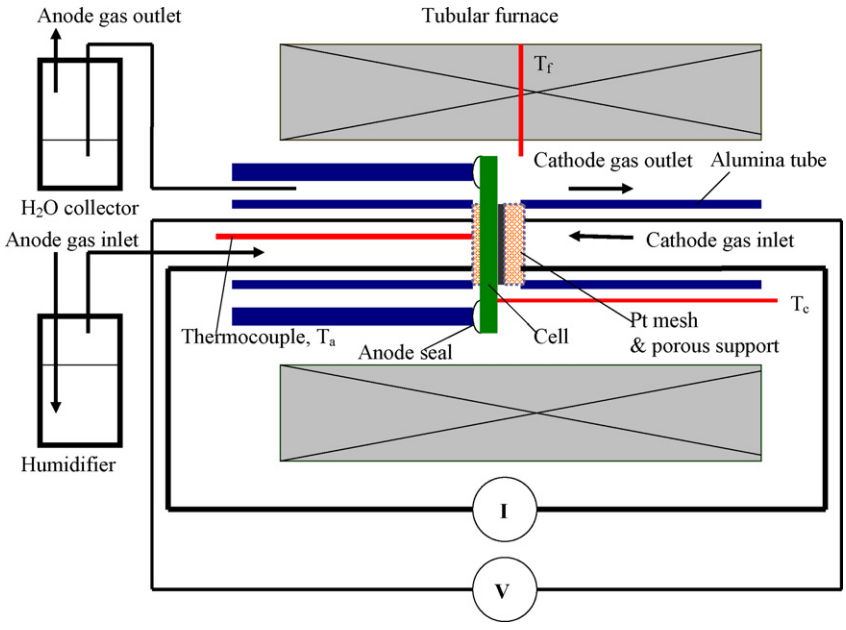

Fig. 2. Schematic of experimental setup.

then connected to a dry container for water collection. Water was collected at each cell test temperature for 20 h. No current was drawn from the cell during water collection, except the test at 600 °C. At 600 °C, conditions both without and with current were tested.

Electrochemical measurements were performed at temperatures ranging from 650 to 500 °C under ambient pressure. Cell performances were measured with a Multi-channel Potentiostat/Galvanostat (Solartron 1480 eight-channel multi-stat) with a computer interface and Corr-view software. The *I–V* curves and power curves were obtained using linear sweep voltammetry at a sweep rate of 4 mV s^{-1} from open circuit voltage (OCV) to 0.3 V. The electrochemical impedance spectra (EIS) were typically measured in the frequency range from 65 kHz to 0.1 Hz with 50 mV perturbation amplitude using a Solartron 1250 FRA and computer interface and Z-view software. The cell resistance (R_{cell}) was calculated using data fitting from the *I–V* curve, and the electrolyte resistance (R_{el}) and electrode polarization resistance (R_p) were calculated using EIS data fitting. The electrochemical measurements were performed before and after water collection.

The morphologies of the tested cells were observed using a scanning electron microscope (SEM, Hitachi S-3500N), coupled with energy dispersive spectrometry (EDS) and X-ray diffraction techniques for elemental and phase analysis, respectively. The SEM sample for cross-section observation was embedded in epoxy resin and polished. Each sample was coated with Au–Pd alloy before observation.

3. Results and discussion

3.1. Cell electrochemical performance

Fig. 3 shows the OCV of the cell in this study at different temperatures along with the Nernst potential (E_N). E_N was calculated based on the temperature and reactant gas composition (97% H_2 + 3% H_2O for anode and 21% O_2 in air for cathode, both at 1 atm), under an assumption that the entropy of the reactants is independent of temperature. The thermodynamic properties of the reactants were sourced from Lange's Handbook (15th edition). Different thicknesses and theoretical OCV of an SDC electrolyte from refs. [4,11,21] are also presented in this figure. As shown in Fig. 3, the recorded OCV value of this study decreased from 0.873 V at 500 °C to 0.796 V at 650 °C. It is well known that electronic conductivity in the SDC electrolyte is increased at high temperatures under anodic fuel conditions, leading to a decrease in OCV at a higher temperature. However, the recorded OCV data in this study were lower than those reported with thick SDC electrolytes. The reported OCVs were 0.98 and 0.94 V at 600 °C for SDC electrolyte-supported cells of SDC electrolyte thicknesses 2.2 and 1.19 mm, respectively

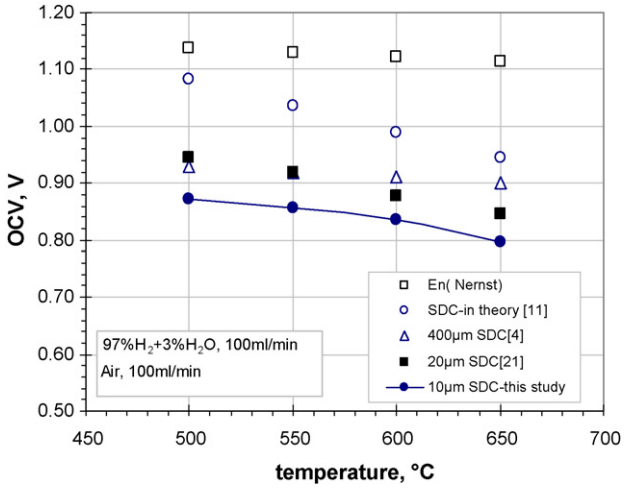

Fig. 3. OCV of the SDC electrolyte cells at different temperatures.

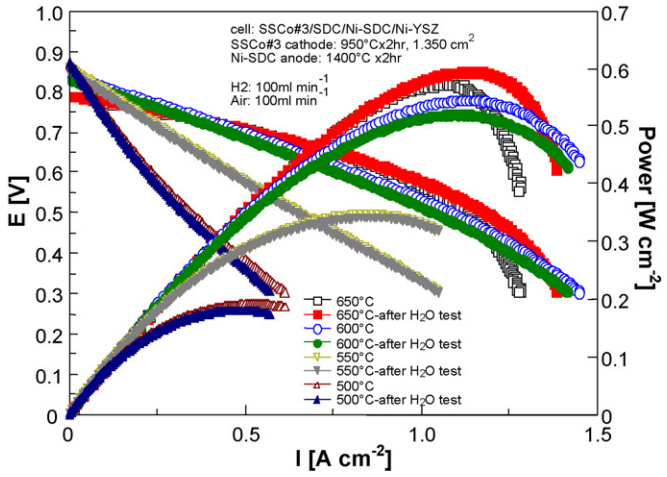

Fig. 4. Cell performance at different temperatures.

[11], and only 0.91 V for a 0.4 mm thick SDC cell [4], 0.87 V for a cermet-supported 20 μm thick SDC cell [21] and 0.835 V for the 10 μm thick SDC electrolyte cell used in this study. The explanation of the variation of OCV with thickness of the SDC electrolyte can be either that fewer defects that span the entire thickness of the thick electrolyte, resulting in higher gas-tightness in the thicker electrolytes, or that the distribution of partial pressure of oxygen inside the electrolyte is thickness-dependent, causing the OCV to decrease with the thickness due to an increase in the electronic conductivity. The widening deviation of the real OCV from the theoretical OCV of the SDC electrolyte at lower temperatures, as shown in Fig. 3, may also result in part from the increasing electrode polarization. As reported by Miyashita [12] and Liu and Hu [13], the electrode polarization also contributes to the total cell voltage loss even at OCV, especially when operating at lower temperature.

Fig. 4 shows the performance of the cell before and after water collection tests at different temperatures. It can be seen that the maximum power densities reached 595 mW cm^{-2} at 650 °C, 545 mW cm^{-2} at 600 °C and 347 mW cm^{-2} at 550 °C. It was noticed that there was less than a 2 °C difference between the cathode temperature (T_c) and the anode temperature (T_a, the temperature set for the cell test). However, a slight increase (at most 5 °C) in both T_a and T_c were observed during the *I–V* curve measurement, which took approximately 2–3 min. It was also noticed that when the hydrogen was first introduced to the anode side for cell reduction, the furnace temperature (T_f) could drop to 10–15 °C lower than before the hydrogen introduction. The temperature deviation was quite obvious, indicating that the cell was generating heat even at the open circuit condition. Fig. 5a and b shows the electrochemical impedance spectra of the cell at different temperatures before and after water collection tests. The performance of the cell is summarized in Tables 2 and 3. The area-specific resistances of the cell (R^*_{cell}) were obtained from the *I–V* curves (Fig. 4) in the linear range from OCV to 0.75 V, and both electrolyte resistance (R_{el}) and electrode polarization resistance ($R_{p,a+c}$, including both anode and cathode) values were obtained from EIS results by using instant data fitting with Corr-view and Z-view software. The cell area-specific resistance from EIS is R_{cell}, which is the sum of R_{el} and $R_{p,a+c}$. It is notable that the sum of R_{cell} is approximately equal to the R^*_{cell} value at the temperatures tested.

3.2. Water amount and leakage current

Fig. 6 shows the water amount and leakage current calculated based on water amount. The leakage current was calculated simply based on Faraday's Law, under an assumption that the water amount collected during 20 h under the OCV condition resulted entirely from the internal shorting of the SDC electrolyte, and that the leakage current was constant over the 20 h test period.

$$I_L = \frac{FW_w}{36000M_w} = 0.1489W_w \quad (1)$$

where I_L is the leakage current [A], F the Faraday's constant, W_w the water amount [g] accumulated during 20 h and M_w is the molecular weight of water.

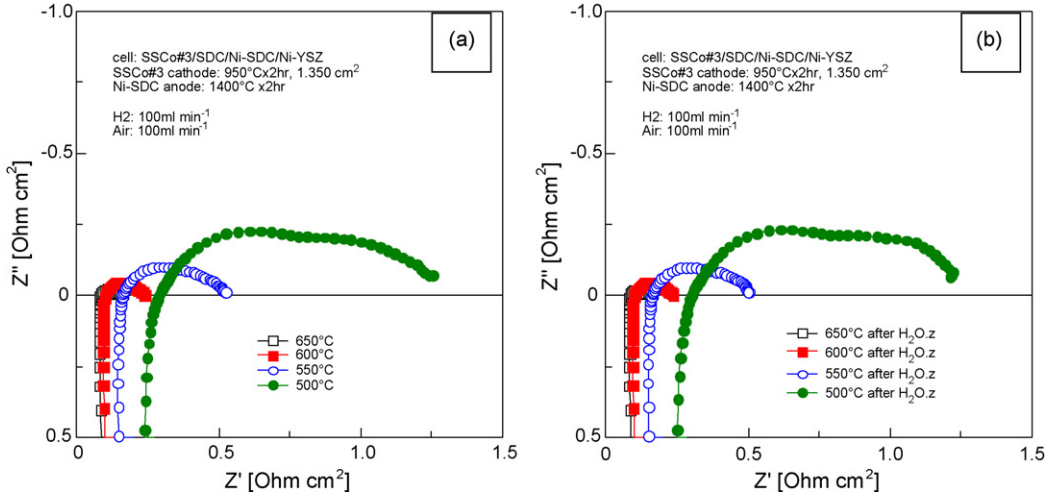

Fig. 5. EIS of the cell at different temperatures: (a) before water test and (b) after water test.

Table 2
Cell performance and EIS results at different temperatures before water test

Temperature [°C]	OCV [V]	MPD [W cm^2]	R_{el} [Ω cm^2]	$R_{p,a+c}$ [Ω cm^2]	R_{cell} [Ω cm^2]	R^*_{cell} [Ω cm^2]
650	0.796	0.575	0.073	0.066	0.139	0.152
600	0.835	0.545	0.099	0.133	0.232	0.265
550	0.857	0.347	0.152	0.361	0.513	0.570
500	0.873	0.193	0.268	0.970	1.238	1.258

OCV, open circuit voltage; MPD, maximum power density; R_{el}, SDC electrolyte ohmic resistance from EIS; $R_{p,a+c}$, electrode electrochemical resistance from EIS; R_{cell}, cell resistance from EIS ($R_{cell} = R_{el} + R_{p,a+c}$); R^*_{cell}, cell resistance from I–V curve (data fitting from OCV to 0.75 V).

Table 3
Cell performance and EIS results at different temperatures after water test

Temperature [°C]	OCV [V]	MPD [W cm^2]	R_{el} [Ω cm^2]	$R_{p,a+c}$ [Ω cm^2]	R_{cell} [Ω cm^2]	R^*_{cell} [Ω cm^2]
650	0.792	0.595	0.071	0.070	0.141	0.156
600	0.831	0.521	0.098	0.130	0.228	0.277
550	0.852	0.341	0.155	0.342	0.496	0.555
500	0.875	0.181	0.282	0.959	1.241	1.336

OCV, open circuit voltage; MPD, maximum power density; R_{el}, SDC electrolyte ohmic resistance from EIS; $R_{p,a+c}$, electrode electrochemical resistance from EIS; R_{cell}, cell resistance from EIS ($R_{cell} = R_{el} + R_{p,a+c}$); R^*_{cell}, cell resistance from I to V curve (data fitting from OCV to 0.75 V).

It can be seen that both the water amount and the leakage current increased with the temperature. Astonishingly, the leakage current of the cell under the open circuit condition reached over 2.26 A at 650 °C and 1.46 A at 600 °C.

To clarify the cathode effect on the internal shorting, a cell from the same batch without a cathode was used for a similar water collection test under open circuit condition. The results of this test are also shown in Fig. 6. It is clear that the water amount and leakage current density are tremendously decreased, reaching only 1/3 of the water amount of the cell with a cathode at 600 °C. This result indicates that the internal shorting is not only dependent on the electronic conductivity of the SDC, but also on the kinetics of the oxygen reduction process. The cathode facilitates the oxygen reduction process and therefore greatly enhances the leakage current under open circuit conditions.

The cell with a cathode was also tested under a constant current density of 0.50 A cm^{-2} (0.675 A) for 20 h at 600 °C.

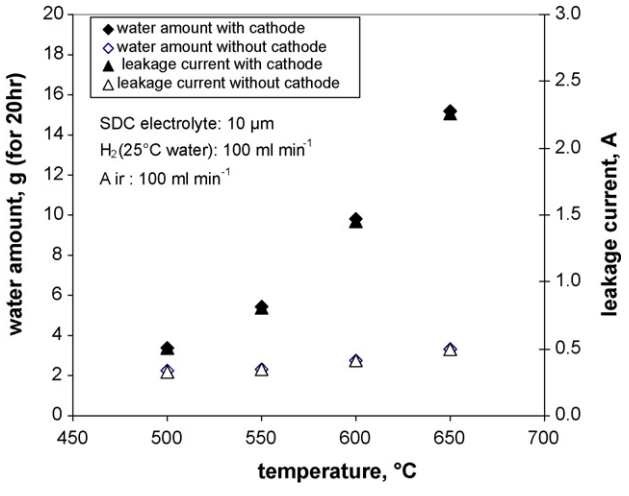

Fig. 6. Water amount collected at anode gas outlet and leakage current at different cell temperatures, with and without the cathode.

The cell voltage under this condition is quite stable, approximately 0.69 V. 11.9746 g water was collected during this period, corresponding to a leakage current of 1.108 A.

In this study, the SDC electrolyte area of the cell without cathode is approximately 5.23 cm^2. The SSCo#3 cathode area was 1.35 cm^2. We assume that the shorting current has two even distributions, one over the portion of the SDC electrolyte without the cathode, and the other over the whole cathode area. Based on Eqs. (1)–(4), the leakage current (I_L) and leakage current density (i_L), both with and without the cathode, can be calculated. The results are listed in Table 4.

$$i^*_L = \frac{I^*_L}{5.23}\ [\mathrm{A\,cm^{-2}}] \tag{2}$$

$$i_c = \frac{I_L - I^*_L}{1.35}\ [\mathrm{A\,cm^{-2}}] \tag{3}$$

$$i_L = i^*_L + i_c\ [\mathrm{A\,cm^{-2}}] \tag{4}$$

where I^*_L and i^*_L are the leakage current and current density without the cathode, I_L and i_L the leakage current and current density with the cathode and i_c is the enhanced leakage current density at the cathode area due to the coverage of the SSCo#3 composite cathode layer. From Table 4, it is clear that with the cathode, the leakage current density was increased almost 10 times in comparison to without the cathode at 600 °C. The leakage current density dropped by up to 30% when the cell was operating at 0.5 A cm^{-2} at 600 °C.

3.3. Internal shorting current density based on OCV deviation

A simple model is derived for the internal shorting current density calculation of the SDC cell, making use of the fact that the electrode overpotential η_s is typically small and linear with

Table 4
Water amount (for 20 h) and leakage current under open circuit condition at different temperatures and at 0.5 A cm^{-2} at 600 °C

Temperature [°C]	W_w [g]	W_w[a] [g]	I_L [A]	I_L^* [A]	i_L^* [A cm^{-2}]	i_c [A cm^{-2}]	i_L [A cm^{-2}]
650	15.174	3.329	2.259	0.496	0.095	1.306	1.401
600	9.788	2.759	1.457	0.411	0.079	0.775	0.854
550	5.407	2.341	0.805	0.349	0.067	0.338	0.405
500	3.369	2.236	0.502	0.332	0.064	0.125	0.189
600[b]	11.975	2.759	1.783	0.411	0.079	1.016	0.595

[a] Without cathode, $i_L = i_L^* + i_c$.
[b] At 0.50 A cm^{-2}, $i_L = i_L^* + i_c - 0.5$.

the current in SOFCs at high temperature operation. In general,

$$E = E_N - i(R_a + R_c + R_{int}) = V_0 - iR_{t,cell} \quad (5a)$$

where E is the cell voltage, E_N the Nernst potential of the cell reaction, i the cell operating current density and R_a and R_c stand for anodic and cathodic polarization resistance, respectively. R_{int} represents the internal ohmic resistance of the cell, which is typically approximated by the electrolyte resistance. $R_{t,cell}$ is the total resistance of the cell. All resistances are expressed as area-specific resistances [Ω cm^2]. Under open circuit condition, Eq. (5a) changes to

$$OCV = E_N - i_L(R_a + R_c + R_{int}) = V_0 - i_L R_{t,cell} \quad (5b)$$

where OCV is the cell open circuit voltage and i_L is the cell leakage current density.

The leakage current density $i_{L,\,calc.}$ was calculated from Eq. (5b) by inserting the OCV value and cell resistance value, $R_{t,cell}$ (an average of the cell resistances R_{cell} and R_{cell}^* in Tables 2 and 3). The results are listed in Table 5. The leakage current density based on the measured water amount, $i_{L,\,meas.}$, is also listed in this table. It can be seen that $i_{L,\,calc.}$ values are higher than $i_{L,\,meas.}$ values, suggesting that the calculated leakage current density will be an overestimate using this simple model. This is due to the simple model neglecting the initial electrochemical overpotential loss of the electrodes. For a higher accuracy of data fitting, one can introduce non-linear Butler–Volmer equations for the electrode over-potential calculations [16]. Here, we simply replace E_N with a parameter V_0 in Eq. (5b) and do the fitting based on the $i_{L,\,meas.}$ value. It was found that the V_0 values are in the range of 1.0–1.1 V. As we know, the V_0 value for a YSZ electrolyte based SOFC is commonly in this range, and no leakage current is observed due to the pure ionic conductivity of YSZ. Sahibzada et al. [18] developed a model to analyze the possible leakage current density of a 10 μm thick $Ga_{0.1}Ce_{0.9}O_{1.95}$ electrolyte anode supported cell. Their calculation showed that i_L at OCV conditions could be as high as 0.610 A cm^{-2} at 600 °C, although they did not experimentally verify their model results. Results in this study clearly indicate that the leakage current densities at the tested conditions are truly measurable and intolerably high. Based on Eq. (5b), one may reach a conclusion that for an SDC electrolyte cell, both the thinner the electrolyte and the higher-performing the electrodes are, the higher the leakage current density will be. A thinner electrolyte will not only reduce the cell resistance (R_{cell}), but also enhance the possibility of electrolyte defects, such as pinholes or cracks, spanning the entire electrolyte thickness, leading to an even lower OCV caused by gas leakage, and thus further decreasing the efficiency and fuel loss in the cell.

3.4. Low electrical efficiency due to internal shorting of the SDC electrolyte

Matsui et al. has calculated that the anode-supported 10 μm SDC electrolyte cell with ideal electrodes (i.e., zero electrode polarization) can reach an electrical efficiency of approximately 61% at a cell voltage of 0.72 V in the same temperature range of this study [17]. In this study, we found that in the case of the cell operating at 0.50 A cm^{-2}, 600 °C, 5% fuel utilization and 12.5% air utilization, the internal shorting current density was 0.60 A cm^{-2}. This means that the fuel loss due to internal shorting is 1.2 times higher than the fuel used for electrical power generation under this operating condition. Since the electronic conductivity of the SDC electrolyte depends on the temperature and anode side oxygen partial pressure, an increase in the fuel utilization will lead to a decrease in electronic conductivity of SDC, and therefore decrease the leakage current density across the electrolyte [16,17]. However, in real operation, the cell voltage will decrease due to increasing fuel utilization. As a result, the cell will operate at a lower efficiency. As indicated in Fig. 7, in this study, for the SDC cell operating at 0.5 A cm^{-2} at 600 °C, an increase in the fuel utilization from 5 to 50% leads to a decrease of the cell voltage from 0.692 to 0.546 V. Further increasing the fuel utilization to over 60% causes a sharp

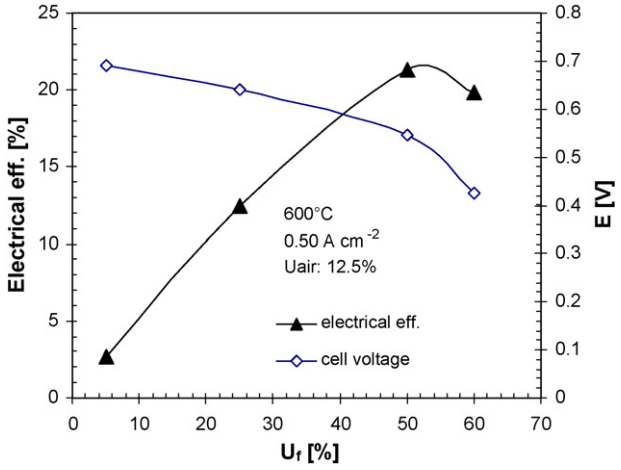

Fig. 7. Fuel utilization (U_f) and electrical efficiency (LHV) of the cell.

Table 5
Leakage current densities based on either OCV value or measured water amount

Temperature [°C]	E_N [V]	OCV [V]	$R_{t,cell}$ [Ω cm^2]	$i_{L,calc.}$ [A cm^{-2}]	$i_{L,meas.}$ [A cm^{-2}]	V_0 [V]
650	1.115	0.796	0.147	2.169	1.401	1.002
600	1.123	0.835	0.250	1.148	0.854	1.049
550	1.130	0.857	0.534	0.512	0.405	1.073
500	1.138	0.873	1.268	0.209	0.189	1.113

E_N, theoretical Nernst cell voltage at the tested condition; OCV, measured cell open circuit voltage; $R_{t,cell}$, average cell resistance value of R_{cell} and R^*_{cell} (see Tables 2 and 3); $i_{L,calc.}$, calculated leakage current density based on Eq. (5b); $i_{L,meas.}$, measured leakage current density based on collected water amount (refer to i_L in Table 4); V_0, fitting parameter based on Eq. (5b).

drop in the cell voltage. The highest electrical efficiency (based on lower heating value) was only 21% at 50% fuel utilization. Accordingly, it seems difficult for the cermet supported, thin SDC electrolyte cell to reach high fuel utilization with high cell performance, due to severe internal shorting, although modeling results had suggested that it should be possible [16,17].

The calculation of the theoretical leakage current density i_L through the electrolyte is rather complex, as it depends on a number of factors [16]:

- The operating temperature, T;
- The oxygen partial pressure distribution across the electrolyte, $p_{O_2,el}$;
- The electronic conductivity of the electrolyte, σ_e, which greatly depends on $p_{O_2,el}$ and T, and can be significantly changed by the presence of impurities at the grain boundaries, or other phase inclusions generated during cell fabrication;
- The ionic conductivity of the electrolyte, σ_i, which can be significantly reduced by the presence of impurities at the grain boundaries, or other phase inclusions generated during cell fabrication;
- The electrode polarization resistance, $R_{p,a+c}$;
- The cell operating current density, i.

It was observed in this study (see Table 4) that the i_L value under 0.5 A cm^{-2} operating current density was smaller than that under open circuit conditions. These i_L values were 0.595 and 0.854 A cm^{-2}, respectively. The effect of an increase in the cell operating current density is that it increases the average oxygen partial pressure in the electrolyte, resulting in a decrease in the σ_e value of the electrolyte, and thus also the i_L. However, the leakage current density under this condition is still over two orders of magnitude higher than that in the modeling result from ref. [16].

3.5. The SDC conductivities in this study

As is widely known, a doped ceria electrolyte behaves as a mixed conductor. The ionic conductivity of SDC (σ_i) is purely a function of temperature, but the electronic conductivity (σ_e) is a function of both temperature and the local oxygen partial pressure (p_{O_2}). The electronic conductivity of SDC is negligible at temperatures below 400 °C and/or in an oxidizing environment [16]. However, the oxygen partial pressure at the anode ($p_{O_2,anode}$) under the conditions of this study is typically in the range of 10^{-25} to 10^{-31} atm, which leads to the SDC electrolyte exhibiting a significant σ_e. The oxygen ionic conductivity (σ_i) and electronic conductivity (σ_e) of the doped-ceria electrolyte can be estimated as

$$\sigma_i = \frac{\sigma_{0,i}}{T} \exp\left(-\frac{E_{a,i}}{RT}\right) \quad (6)$$

$$\sigma_e = \sigma_{0,e} \frac{(p_{O_2,el})^{-1/4}}{T} \exp\left(-\frac{E_{a,e}}{RT}\right) \quad (7)$$

For $Ga_{0.1}Ce_{0.9}O_{1.95}$ [18], $\sigma_{0,i} = 2.706 \times 10^6$ [S K m^{-1}], $E_{a,i} = 61.748 \times 10^3$ [J mol^{-1}]; $\sigma_{0,e} = 2.342 \times 10^{11}$ [S K atm$^{1/4}$ m^{-1}], $E_{a,e} = 238.78 \times 10^3$ [J mol^{-1}]. In this study, based on the measured R_{el} value and assuming that the resistance comes solely from the ionic conductivity of the 10 μm thick SDC electrolyte (thickness δ_{el}), we obtain $\sigma_{0,i} = 4.3045 \times 10^6$ [S K m^{-1}], $E_{a,i} = 61.89 \times 10^3$ [J mol^{-1}].

The electronic and ionic conductivities can be obtained through the ionic transference number (t_i), and the total conductivity (σ_t) of the electrolyte as measured. t_i and σ_t were calculated from Eqs. (8) and (9) [13,19], under an assumption that no influence on the cell OCV value comes from electrode polarizations in this study. The calculated σ_e and σ_i values at different temperatures are listed in Table 6.

$$t_i = \frac{OCV}{E_N} \quad (8)$$

$$\sigma_t = \frac{\delta_{el}}{R_{cell}} \quad (9)$$

$$\sigma_i = t_i \sigma_t \quad (10)$$

$$\sigma_e = (1 - t_i)\sigma_t \quad (11)$$

It is worth mentioning that the calculated σ_e is related to the oxygen partial pressure within the electrolyte. For simplicity, the values of both $\sigma_{0,e}$ and $E_{a,e}$ in Table 6 were obtained by assuming that the $p_{O_2,el} = 0.21$ atm, the highest value in the electrolyte (cathode side), for Eq. (7).

As listed in Table 6, the reported conductivities (σ_i) of SDC ($Sm_{0.2}Ce_{0.8}O_{1.9}$) can be as high as 3.0 S m^{-1} at 650 °C and 2.0 S m^{-1} at 600 °C [14,15]. The measured σ_i value in this study was only about 1/3 to 1/2 of the reported σ_i value at the test temperature, implying that certain detrimental interactions might have taken place in the SDC electrolyte during the cell processing. The measured σ_i of the SDC in this study was slightly higher than that of GDC ($Gd_{0.1}Ce_{0.9}O_{1.95}$), and the activation energy (E_a), 61.75 kJ mol^{-1} was very close to that of GDC reported in ref. [18].

Table 6
The conductivities of the SDC (GDC) electrolytes [14,15,18]

T [°C]	500	550	600	650	σ_o [S K cm^{-1}]	E_a [kJ mol^{-1}]	Reference
$\sigma_{i,\,SDC}$ [S m^{-1}]	0.59	1.16	1.92	3.01	302549	71.19	[14]
	0.66	1.25	2.08	3.20	255250	69.42	[15]
$\sigma_{i,\,GDC}$ [S m^{-1}]	0.24	0.40	0.63	0.94	27174	61.75	[18]
$\sigma_{t,\,GDC}$ [S m^{-1}]	0.355	0.649	1.019	1.415	43045	61.89	This
$\sigma_{i,\,SDC}$ [S m^{-1}]	0.272	0.490	0.758	1.010	21807	61.75	study
$\sigma_{e,\,SDC}$ [S m^{-1}]	0.083	0.156	0.261	0.405	34132	69.87	

3.6. Cathode contribution

The oxygen reduction process at the cathode includes diffusion, adsorption, dissociation, charge transfer and oxygen ion dissolution into the SDC electrolyte. The leakage current density on the bare SDC electrolyte is much smaller than that in the SDC covered with a cathode (see Table 4 and Fig. 6). The apparent activation energies ($E_{a,or}$) of oxygen reduction in both cases are quite different, 15.96 kJ mol^{-1} for without cathode and 80.39 kJ mol^{-1} for with cathode, indicating that the oxygen reduction mechanism was different. Although the bare SDC surface shows a certain catalytic function in oxygen reduction, the rate-determining step of oxygen reduction is most likely the dissociation of oxygen or surface diffusion of oxygen species, or a combination of the two. With the cathode present, the processes of adsorption and dissociation of oxygen are greatly enhanced by the higher effective surface area and catalytic role of the SSCo cathode. With sufficient cathode activity and reaction area, the rate-determining step shifts to the oxygen ion generation, dissolution and transport in the electrolyte. In the case of an ideal cathode at OCV, the oxygen reduction process will be completely controlled by both the electronic and the ionic conductivities of the electrolyte.

3.7. Cell microstructure and EDS analysis

Figs. 8 and 9 show plane and cross-section views of the tested cell, including EDS analyses of the electrolytes. Although the SDC surface appears nearly fully dense with very few pinholes, many irregular grains on the SDC electrolyte surface were observed after the 1400 °C—2 h co-firing and prior to cathode deposition (Fig. 8a). The cell cross-section reveals some defects existing in the electrolyte, which may be one of the contributing factors to the slightly lower OCV observed in this study compared to that of thicker SDC electrolytes reported previously in the lierature. Fig. 9 shows the EDS analysis results of a regular grain and an irregular grain in Fig. 8a, marked with #1 and #2, respectively. EDS analysis results show that the irregular grains have a high Zr content, and have the appearance of micro-islands, so they are referred to as Zr-micro-islands in the present work. The cross-section of the SDC electrolyte after sample polishing also reveals Zr content inclusions.

It can be seen from the composition tables in Fig. 9 that the irregular grain shows not only a high Zr content, but also an enriched Sm content, while the Ce content is substantially decreased. This result suggests that either Zr has replaced some of the Ce atoms on the Ce sites in the normal SDC lattice, or that a second Sm-rich phase containing Zr separates from the SDC phase. High Sm content in the irregular grain indicates that Sm has a higher solubility in those grains than in the bulk. Furthermore, since the grain size of the Zr-island is larger than that of the normal SDC grains, this second phase likely also has a higher vapour pressure or lower melting point, a faster grain growth rate, and higher sinterability than that of normal SDC during the cell co-firing. The high Sm content in the

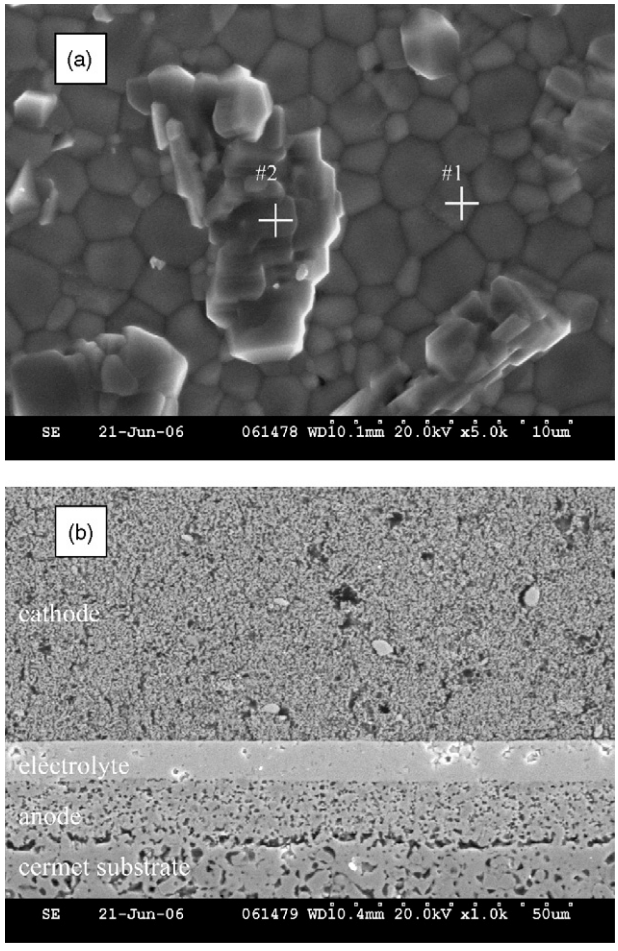

Fig. 8. SEM images of the SDC electrolyte after cell test: (a) SDC electrolyte surface and (b) cell cross-section.

Table 7
Ionic conductivity (σ_i) and electronic conductivity (σ_e) of YSZ, GDC and their mixed composites at 800 °C in air [20]

Material	Nominal composition	σ_i [S m^{-1}]	σ_e [S m^{-1}]
YSZ	$Zr_{0.85}Y_{0.15}O_{1.93}$	5.4	7.29×10^{-11}
GDC	$Ce_{0.80}Gd_{0.20}O_{1.90}$	8.7	8.18×10^{-4}
Reaction product	$Ce_{0.37}Zr_{0.38}$ $Gd_{0.18}Y_{0.07}O_{1.87}$	0.125	3.99×10^{-4}
Interlayer	$Ce_{0.43}Zr_{0.43}$ $Gd_{0.10}Y_{0.04}O_{1.93}$	0.603	3.88×10^{-4}

irregular grains also suggests that the depletion of Sm-dopant from the bulk SDC composition has occurred, which could be one of the reasons for the low ionic conductivity (σ_i) in this study.

The Zr-micro-islands are potentially detrimental to the cell performance. Tsoga et al. [20] reported that the Zr–Ce–Gd–Y–O composite phase exhibits a conductivity two orders of magnitude lower than that of GDC. Table 7 lists their conductivity data, recorded at 800 °C. Since Sm-doped ceria and Gd-doped ceria have very similar conductivities, it is likely that the Zr-micro-islands observed in this work may also consist of a very low conductivity phase, based on the analyzed compositions, and their similarity with the compositions studied by Tsoga et al. Simply based on the σ_e/σ_i ratios in Table 7, it is noticed that the ratio of the electronic to ionic conductivity of the composite phase could be increased 7–35 times in comparison to that of the pure GDC, which means that the inclusions found in this study might contribute to a lower OCV. The formation of Zr-micro-islands is likely related to Zr migration from the NiO–YSZ substrate during the co-firing process [21].

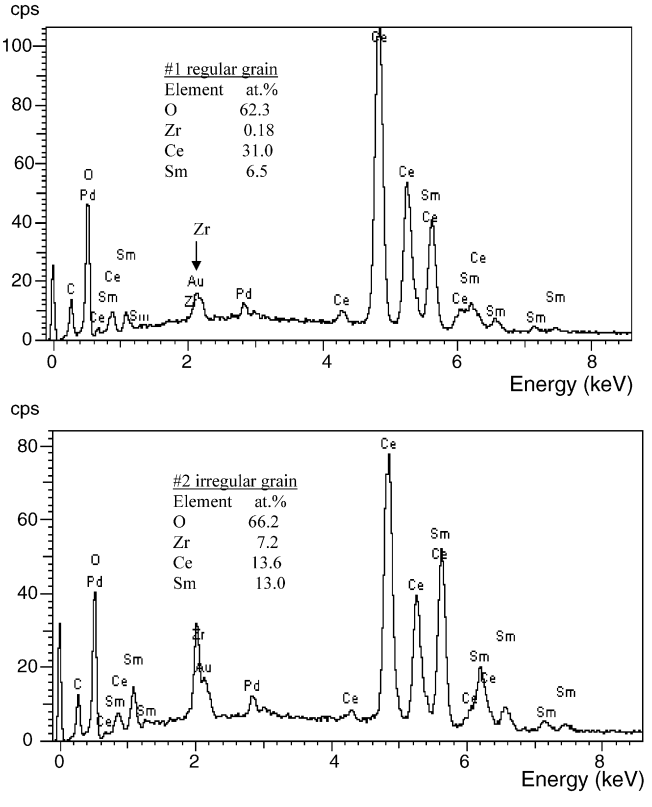

Fig. 9. EDS analysis results at regular grain and irregular grain on the SDC electrolyte surface after co-firing (see Fig. 8a).

4. Conclusions

Thin film (10 μm) SDC electrolytes have been co-fired on porous NiO–SDC anodes with NiO–YSZ substrates. The SDC electrolyte cells, with and without cathodes, were tested in the temperature range of 500–650 °C. The cell with an SSCo–SDC composite cathode showed a high electrochemical performance at temperatures ranging from 500 to 650 °C. A peak power density of 595 mW cm^{-2} at 650 °C was obtained. However, the cell exhibited severe internal shorting due to the mixed conductivity of the SDC electrolyte. Both the amount of water collected from the anode outlet and the open circuit voltage value indicated that the internal shorting current could reach 0.85 A cm^{-2} or higher at 600 °C. The SSCo–SDC composite cathode plays a key role in a fast oxygen reduction process, and in the intolerable internal shorting under OCV conditions observed in this study. A simple model was developed for the internal leakage current calculation. It appears that both higher electrode performance and thinner electrolytes lead to higher leakage currents in a thin SDC electrolyte cell. Zr content inclusions were found at the surface and the cross-section of the SDC electrolyte, which could be one of the reasons for reduced OCV and lower oxygen ionic conductivity. Fuel loss due to internal shorting of the thin SDC electrolyte cell becomes a substantial concern for its use in applications requiring high fuel utilization and electrical efficiency. Future developments will require minimising the electronic leakage current either by doped-ceria electrolyte composition modification or by deposition of electronic blocking layers to control the level of the electronic conductivity of the whole electrolyte layer.

Acknowledgement

The authors would like to thank the National Research Council of Canada for supporting the low temperature SOFC project.

References

[1] S. de Souza, S.J. Visco, L.C. de Jonghe, Solid State Ionics 98 (1997) 57.
[2] Z. Yang, K.S. Weil, D.M. Paxton, J.W. Stevenson, J. Electrochem. Soc. 150 (2003) A1188–A1201.
[3] W.Z. Zhu, S.C. Deevi, Mater. Res. Bull. 38 (2003) 957.
[4] C. Xia, W. Rauch, F. Chen, M. Liu, Solid State Ionics 149 (2002) 11.
[5] S. Zha, W. Rauch, M. Liu, Solid State Ionics 166 (2004) 241.

[6] G. Schiller, R. Henne, M. Lang, S. Schaper, Development of metallic substrate supported thin-film SOFC by applying plasma spay techniques, in: Proceedings of SOFC VI, Electrochemical Society, 1999, pp. 893–903.
[7] N.P. Brandon, A. Blake, D. Corcoran, D. Cumming, A. Duckett, K. El-Koury, D. Haigh, C. Kidd, R. Leah, G. Lewis, C. Matthews, N. Maynard, N. Oishi, T. McColm, R. Trezona, A. Selcuk, M. Schmidt, L. Verdugo, J. Fuel Cell Sci. Technol. 1 (November) (2004) 61.
[8] S. Zha, A. Moore, H. Abernathy, M. Liu, J. Electrochem. Soc. 151 (2004) A1128–A1133.
[9] W. Wang, M. Mogensen, Solid State Ionics 176 (2005) 457.
[10] Z. Shao, S.M. Haile, Nature 431 (2004) 170.
[11] T. Matsui, T. Kosaka, M. Inaba, A. Mineshige, Z. Ogumi, Solid State Ionics 176 (2005) 663.
[12] T. Miyashita, J. Mater. Sci. 41 (2006) 3183.
[13] M. Liu, H. Hu, J. Eletrochem. Soc. 143 (1996) L109.
[14] V.V. Kharton, F.M.B. Marques, A. Atkinson, Solid State Ionics 174 (2004) 135.
[15] S.P.S. Badwal, Solid State Ionics 52 (1992) 23.
[16] R.T. Leah, N.P. Brandon, P. Aguiar, J. Power Sources 145 (2005) 336.
[17] T. Matsui, M. Inaba, A. Mineshige, Z. Ogumi, Solid State Ionics 176 (2005) 647.
[18] M. Sahibzada, R.A. Rudkin, B.C.H. Steele, I.S. Metcalfe, J.A. Kilner, in: U. Stimming, et al. (Eds.), SOFC V Proceedings, vol. 97–40, Electrochemical Society, NJ, 1997, p. 244.
[19] H. Iwahara, Solid State Ionics 52 (1992) 99.
[20] A. Tsoga, A. Naoumidis, D. Stover, Solid State Ionics 135 (2000) 403.
[21] X. Zhang, M. Robertson, et al., J. Power Sources 161 (2006) 301.